minerals

MDPI

Article

Lysozyme–Mineral Clay Systems: Comparison of Interaction for Controlled Release in Feed Application

Marianna Guagliano [1,*], Matteo Dell'Anno [2], Giovanni Dotelli [1], Elisabetta Finocchio [3], Maria Lacalamita [4], Ernesto Mesto [4], Serena Reggi [2], Luciana Rossi [2], Emanuela Schingaro [4], Elena Staltari [1] and Cinzia Cristiani [1,*]

[1] Dipartimento di Chimica, Materiali e Ingegneria Chimica "Giulio Natta", Politecnico di Milano, Piazza Leonardo Da Vinci 32, 20133 Milano, Italy; giovanni.dotelli@polimi.it (G.D.); elena.staltari@mail.polimi.it (E.St.)
[2] Dipartimento di Medicina Veterinaria e Scienze Animali—DIVAS, Università Degli Studi di Milano, Via dell'Università 6, 26900 Lodi, Italy; matteo.dellanno@unimi.it (M.D.); serena.reggi@unimi.it (S.R.); luciana.rossi@unimi.it (L.R.)
[3] Dipartimento di Ingegneria Civile, Chimica e Ambientale, Università di Genova, Via Opera Pia 15, 16145 Genova, Italy; elisabetta.finocchio@unige.it
[4] Dipartimento di Scienze Della Terra e Geoambientali, Università Degli Studi di Bari Aldo Moro, Via Edoardo Orabona, 4, 70125 Bari, Italy; maria.lacalamita@uniba.it (M.L.); ernesto.mesto@uniba.it (E.M.); emanuela.schingaro@uniba.it (E.S.)
* Correspondence: marianna.guagliano@polimi.it (M.G.); cinzia.cristiani@polimi.it (C.C.)

Abstract: A synthetic approach to bond lysozyme (LY) to commercial natural carriers, namely clay minerals (bentonite, BN; and sepiolite, SP) and commercial zeolite (Phil 75®, PH), already in use in feed formulation, is proposed. The synthetic route, which implies solid–liquid adsorption, is a simple and effective way for preparing hybrid materials characterized by LY loadings up to 37 $mg_{LY}/g_{carrier}$. By operating at pH 4.3, initial LY content of 37.5 $mg_{LY}/g_{carrier}$, and reaction time of 90 min, hybrid materials with LY loadings of 37, 35, and 12 $mg_{LY}/g_{carrier}$ for LY-SP, LY-BN, and LY-PH, respectively were obtained. The LY initial concentration and pH, as well as the physico-chemical properties of the carries were found to be the parameters that govern the synthesis of the materials. The driving force for an effective LY adsorption and interaction is the combined Zero Point Charge (ZPC) of the carriers, always negative (in the range between −4 and −170 mV) and the positive ZPC of LY, as well as the carrier morphology, characterized by mesoporosity (pore dimensions in the range of 5–12 nm). However, it is the interaction of charges of opposite sign that mainly affects LY loadings and bond strength. Based on SEM-EDX analysis, LY molecules are quite homogeneously spread onto the carriers' surface. TG-DTG analyses showed that the LY–carrier interaction in the hybrid materials is stronger than that in a simple mechanical mixture of the components. Specifically, in the hybrid materials, the phenomenon at 300 °C, associated to LY decomposition, is broadened and slightly shifted towards higher temperatures (320–350 °C), whereas in a mechanical mixture of the same composition, it occurs at temperatures closer to those of free LY, as if there were no or very weak interactions. At pH 3, a very little LY release, 0.03 and 0.01 $mg_{LY}/g_{carrier}$, was found for LY-BN and LY-PH, respectively. The latter became larger at pH 7, 0.06 $mg_{LY}/g_{carrier}$ for both BN and PH carriers, suggesting that BN and PH are better modulators of LY release. The paper provides insights for the study and the development of new optimized feed formulations for the targeted delivery of natural compounds with antimicrobial activity, alternatives to antibiotics, and vaccinal antigens.

Keywords: lysozyme controlled release; clay minerals and zeolite; solid–liquid adsorption; feed application; material characterization

Citation: Guagliano, M.; Dell'Anno, M.; Dotelli, G.; Finocchio, E.; Lacalamita, M.; Mesto, E.; Reggi, S.; Rossi, L.; Schingaro, E.; Staltari, E.; et al. Lysozyme–Mineral Clay Systems: Comparison of Interaction for Controlled Release in Feed Application. *Minerals* **2023**, *13*, 660. https://doi.org/10.3390/min13050660

Academic Editors: Michal Slaný and Itamar Shabtai

Received: 6 April 2023
Revised: 6 May 2023
Accepted: 8 May 2023
Published: 10 May 2023

1. Introduction

Proteins absorbed on solid surfaces have potentially wide fields of applications in biology, medicine, biotechnology, and food processing. A specific protein adsorbed onto proper

materials surface is considered strategical for surface engineering, when antibacterial, or edible coatings is the target [1].

Feed additives fall in these fields of application, consisting of several products, such as bioactive molecules, microorganisms, and inorganic substances. Their use is aimed to improve animals' health and growth, because they promote ingestion, adsorption, and assimilation of the nutrients [2]. In accordance with article 6 of the EC No. 1831/2003 regulation, they can be classified in five main categories: technological, organoleptic, nutritional, zootechnics, coccidiostats, and histomonostats [3]. Among them, technological additives, such as minerals, are gaining a lot of attention, because they can improve handling or hygiene characteristics of the feed [4].

In this respect, one of the main challenges in the oral delivery of biomolecules is the gastric passage [5], and additive protection has been proposed as a viable solution to bypass the problem. Different protection approaches have been proposed [6], and among others, natural carriers, such as natural clays or zeolite, have been reported as a viable route [7]. Clay minerals and zeolite are already exploited in feed technology because of their high adsorption capacity, swelling capacity, safety for animal health, and low cost [4]. Bentonite (E558), sepiolite (E562), and zeolites such as Phil 75® (E566) are commonly added to animal feed to reduce mycotoxin contamination, thus preventing their adsorption in the gastrointestinal tract [3]. Accordingly, their morphological and physico-chemical characteristics make them potentially suitable as solid sorbents and carriers for bioactive molecules in zootechnical applications.

Interactions between bioactive molecules, such as lysozymes, and clay minerals are an important topic, and many reports on type and strength of bonds, proteins conformation, and allocation can be found in the open literature [1,8–11]. For instance, using atomistic molecular dynamics simulations, Kubiak-Ossowska et al. [8] assessed the adsorption of hen egg white lysozyme at a model charged surface, while the lysozyme−smectite systems in water solutions were studied by atomic force microscopy [1]. Similarly, via a molecular dynamic simulation approach, the protein-binding mechanism on montmorillonite and kaolinite was studied [9]. Furthermore, based on Langmuir model isotherms, the influence of the interlayer cation on the maximum protein adsorption has been reported [10]. However, a large part of the studies has been performed either on clay model systems, or on the theoretical calculation and modelling of the protein–carrier interaction. Therefore, despite substantial good work on this subject, to the authors' knowledge, little has been carried out on commercial systems or on materials which are closer to the in-field application. The study of commercially applied carriers, generally complex mixtures characterized by very low purity, is of fundamental importance to find a close connection between the feed additive composition and their effectiveness when applied to a real case, for instance weaned pigs farming.

Nowadays, nutrition sciences target enhanced animal health using feed additives with extra-nutritional value as alternatives to antimicrobials to cope with the increasing problem of antimicrobial resistance [12]. The target delivery of antimicrobial compound or vaccine antigens should be considered for the future sustainable development of precision livestock farming. The demand for new and more effective treatments is increasing since several drugs have become ineffective against specific viruses or bacteria due to the development of resistance mechanisms [13]. Oral administration of vaccines and natural compound alternatives to antibiotics have the potential to greatly cut the cost of farming and promote the environmental sustainability of livestock [14–17].

Lysozyme is well known for its antimicrobial activity mainly against Gram-positive bacteria, thus hampering the bacterial growth [18–20]. Previous studies showed that the dietary supplementation of lysozyme could enhance gastrointestinal health, metabolic profile, and modulate gastrointestinal bacteria ecology of swine [21].

For these reasons, in this work, commercial clay minerals such as Ca-bentonite and sepiolite, as well as Phil 75®, have been studied as examples of carriers already applied in the market, while lysozyme has been chosen as model of bioactive molecule. The final goal

is the evaluation of clays and zeolite as possible carriers for functional feed additives, and alternatives to antimicrobial substances or vaccines.

Accordingly, hybrid materials, consisting of the lysozyme bonded to the inorganic carriers, have been prepared via a solid/liquid adsorption reaction in aqueous environment. This process has already been reported to be easy, environmentally friendly, and cost effective [7,22].

The experimental approach, and the operating conditions for an effective lysozyme loading onto the carriers have been assessed; in particular, reaction time, lysozyme concentration, and pH were the parameters of interest. An attempt to evaluate the protein–carrier interactions has also been made. The obtained hybrid materials have been characterized with the combination of XRPD, FT-IR, TG-DTG, and SEM-EDX, with the final goal of obtaining information on the nature and the strength of lysozyme–carrier interactions.

In addition, to simulate the gastrointestinal tract transit in weaned pigs, release tests at different pHs were also performed to quantify and analyze the hybrid materials' release capability and behavior.

It is the authors' opinion that the novelty of this work stands in the study of compounds prepared with commercial carriers, already used in the feed industry as additives, thus, making these materials closer to those commonly present in the market.

Finally, this work proposes a simple preparation route and an equally simple key to understand the interaction phenomena between the bioactive molecule and the carrier. This approach could facilitate the choice of the most appropriate carrier, based on objective data, such as the carrier morphology or the carrier Zero Point Charge. Therefore, this study can constitute a step forward in the development of new optimized feed formulations for the targeted delivery of natural compound alternatives to antibiotics and vaccinal antigens.

2. Materials and Methods

2.1. LY–Carrier Synthesis Procedure

Chicken egg white lysozyme (LY) (E.C.3.2.17, N-acetyl-muramic-hydrolase, supplied by Sigma Aldrich, in powder form, 99.9% pure), was used. It consists of a single polypeptide chain of molecular weight of approximately 14.4 kDa, and is characterized by an isoelectric point (IP) of 11.35.

Bentonite (BN), sepiolite (SP) and Phil 75® (PH) (supplied by Biomicron s.r.l. Reggio Emilia, RE, Italy) were selected as LY carriers.

Pure HNO_3, NaOH (both by Sigma Aldrich, St. Louis, MO, USA, 98% pure), and distilled water were used.

The adsorption of LY was carried out following a previously developed solid–liquid procedure [7], sketched in Figure 1, and summarized as follows:

(a) LY (in the range of 0.25–1.5 mg/mL) was dissolved in 50 mL of demineralized water, at room temperature under magnetic stirring (500 rpm). During the experiments, the pH solution was monitored by a Mettler Toledo FE20/EL20 digital pH-meter (Mettler Toledo, Milano, MI, Italy), and pH values in the range of 3.8–4.5 were measured for all the LY concentrations.

(b) A total of 2 g of pristine carriers were added to the LY solution, and the obtained suspensions were magnetically stirred at 500 rpm and room temperature for the fixed time.

(c) The pH of the suspension was monitored, but not corrected, during the entire time of the experiments. After that, the solids and the liquids were separated by centrifugation at 2451 relative centrifugal force (RCF) for 30 min (32A RotoFix centrifuge, Hettich Italia, Milano, MI, Italy), and supernatants were stored at 4 °C for further analysis.

The effect of initial LY concentration, in the range of 0.25–1.5 mg/mL (i.e., 6.25–37.5 mg_{LY}/g_{AD}) was assessed. The concentration range was selected to reach a final LY loading of about 37–38 $mg_{LY}/g_{carrier}$, which is reported in the literature to properly supply 100 mg_{LY}/kg in the feed [21].

In addition, both reaction time, in the range of 10–90 min, and solution pH in the range of 2–11.3, i.e., at values far, intermediate, and near to the LY IP, were studied.

Mechanical mixtures (MM) were also prepared by contacting, in a mortar, 2 g of carrier (BN, SP, and PH) and an LY solution (1.5 mg/mL), to reach MM of LY loading equal to those of the hybrid materials.

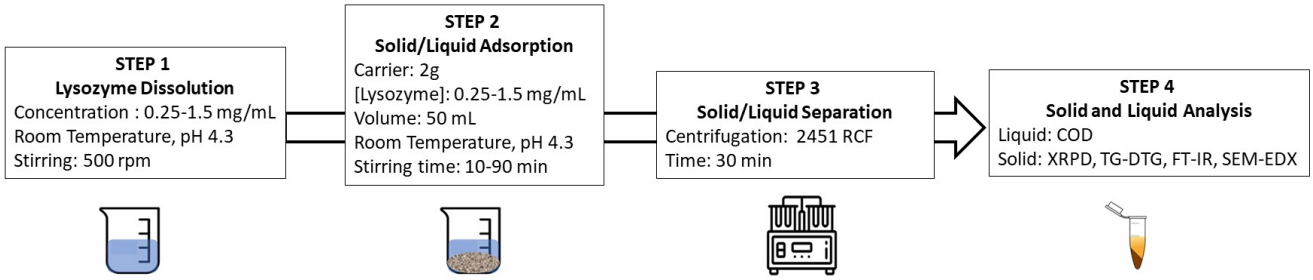

Figure 1. Steps in the solid-liquid adsorption process, (COD: Chemical Oxygen Demand, XRPD: X-ray powder diffraction, TG-DTG: thermogravimetry–derivative thermogravimetry, FT-IR: Fourier-transform infrared, SEM-EDX: scanning electron microscopy and energy dispersive X-ray).

2.2. Characterization

Adsorbed LY was determined by Chemical Oxygen Demand (COD) analysis of the solutions before and after the uptake experiments (HI80 Spectrophotometer, Hanna Instruments, Woonsocket, RI, USA) according to the literature [23,24]. Before the analysis, the liquid samples were digested at 150 °C in a thermoreactor (HI 839,800 Cod Reactor) for 2 h, while the analysis was performed at room temperature.

A calibration curve was used to determine LY values, while the adsorbed LY was calculated by the difference between initial and final LY in solutions according to Equation (1):

$$\text{Adsorbed LY (mgLY/gCarrier)} = [\text{Ini LY (mgLY/gCarrier)} - \text{Res LY (mgLY/gCarrier)}] \quad (1)$$

where "Adsorbed LY" is the amount of captured lysozyme, and "Ini LY" and "Res LY" are the amount of lysozyme in solution before and after the uptake reaction, respectively.

Pristine carriers and hybrid materials were analyzed by several physico-chemical techniques.

Particle dimensions were determined by laser granulometry (CILAS 1180 granulometer, Orléans, France), according to the literature [25,26].

For the morphological analysis, nitrogen adsorption (bath temperature 77.35 K, by a Micromeritics Tristar 3000 instrument, Micromeritics, Norcross, GA, USA), and Hg intrusion (by Autopore V9600 equipment, Micromeritics Instrument Corporation, Norcross, GA, USA) were used; an overnight degassing at 60 °C (heating rate from 25 °C to 60 °C, 1 °C/min) was applied before the analysis.

Solid phase characterization was accomplished by X-ray powder diffraction (XRPD). A Panalytical Empyrean X-ray diffractometer with Bragg–Brentano geometry (Malvern Panalytical Ltd., Malvern, UK) was employed. The instrument, operating at 40 kV/40 mA, is equipped with a large Nickel-beta filter, Cu$K\alpha$ radiation, and a PIXcel3D detector. The powder patterns were collected in the 2θ range of 2–70° with step size 0.0263° and counting time 356 s/step. The PANalytical B.V. software HIGHScore Plus version 4.6a based on the ICSD database (FIZ Karlsruhe, ICSD web v.2.1.0) was used for the phase identification.

Thermal decomposition was analyzed by thermogravimetric and differential thermogravimetric Analysis (TG-DTG) with a DTA-TG SEIKO 6300 instrument (Seiko Instruments Inc., Chiba, Japan), from room temperature up to 800 °C, in air under heating rate of 5 °C/min.

Fourier-transform Infrared (FTIR) spectra were collected in the range of 4000–500 cm^{-1} by a Thermonicolet Nexus (Thermofisher, Waltham, MA, USA), equipped with an Atten-

uated Total Reflection (ATR) accessory (diamond window), 100 scans for each analysis, 4 cm^{-1} resolution, and OMINC software for spectra analysis.

Zero Point Charge (ZPC) was determined by a Zetasizer Nano ZS (Malvern Instruments Limited, Malvern, Worcestershire, UK). The measurement was performed via Dynamic Light Scattering (DLS) at 90°, with a Non-Invasive Backscatter (NIBS) optics.

Scanning electron microscopy and energy dispersion X-ray spectroscopy (SEM-EDX) analysis was performed by a Zeiss EVO 50 EP (Zeiss, Jena, Germany) combined with a spectrometer Oxford INCA energy 2000 (Oxford Instruments, Abingdon, UK).

The SEM-EDX equipment was operated at an electron high tension (EHT) voltage of 15 and 20 kV, a current probe of 120 and 300 pA, and at high vacuum (about 10.4 Pa) to acquire images from both secondary and backscattered electrons as well as for chemical mapping.

Lysozyme Release Assay

Lysozyme release of both the hybrid samples and the mechanical mixture was quantified by indirect competitive enzyme-linked immunosorbent assay (IC-ELISA, plate reader BIORAD, Hercules, CA, USA), which implies the contemporary reading of the samples and proper standards in 96-microwell plates. The process implies a number of steps, sketched in Figure 2, and summarized as follows:

Step 1—Lysozyme Release.

A simulation of lysozyme release was performed at different pHs, simulating gastric and intestinal environments. Briefly, 200 mg of each LY–carrier sample, both hybrid samples and mechanical mixtures, were added to 400 µL of a solution of 10 mM hydroxymethylaminomethane hydrochloric acid (TRIS®, Sigma Aldrich, St. Louis, MO, USA) at pH 3, pH 5, and pH 7. The mixture was then shaken in a rotatory shaker at 180 revolutions per minute (rpm) for 2 h at 37 °C. Subsequently, the supernatant was separated by centrifugation at 16,128 relative centrifugal force (RCF) for 10 min. The liquid extracts were stored at −20 °C until the next assay.

Step 2—ELISA Preparation: Lysozyme standards preparation and microwell plate coating.

Egg hen white lysozyme (Sigma Aldrich, St. Louis, MO, USA) was coated (350 µg/mL in a solution of $CaCO_3$ 50 mM) onto a 96-microwell plate, incubating the plate at 4 °C overnight. Then the plate was washed three times with 0.01 M of Phosphate Buffered Saline (PBS; Sigma Aldrich, St. Louis, MO, USA) at pH 7, then coated with 200 µL of 1% (w/v) Bovine Serum Albumin (BSA, Sigma Aldrich, St. Louis, MO, USA) and incubated for 2 h at 37 °C. The plate was then washed with a solution (PBS-T, in the following) containing 0.01 M PBS and 0.05% (v/v) TWEEN 20® (Sigma-Aldrich, CAS No. 9005-64-5), as described below. The standard curve was obtained using recombinant egg hen white lysozyme (Sigma Aldrich, St. Louis, MO, USA). Six standards were created with different LY concentrations in the range of 0–20 mg/mL, by resuspending the protein in 10 mM TRIS at pH 7 and treating them with the same sample procedure.

Step 3—LY Release Evaluation.

A total of 100 µL of mouse polyclonal anti-lysozyme antibody (Santa Cruz Biotechnology, San Juan, CA, USA), diluted 1:3000, was mixed with 100 µL of the centrifugated liquid from samples and standards (testing each sample in triplicate). Then, 100 µL of all the solutions obtained as previously described, were added to the well-coated plates, then the plates were incubated at 37 °C for 1 h. After incubation, plates were washed with the PBS-T solution first, and then added with 100 µL of a solution 1:10,000 of anti-mouse Immunoglobulin G Horseradish Peroxidase-conjugated (IgG-HRP) antibody (Sigma Aldrich, St. Louis, MO, USA), followed by incubation at 37 °C for 1 h. After, the plates were washed again with the PBS-T solution, and with 50 µL of 3,3′,5,5-tetramethylbenzidine (TMB Sigma Aldrich, St. Louis, MO, USA) and incubated again at 37 °C for 15 min. To stop the peroxidase reaction, 150 µL of a solution 0.4 M in HCl were added to each well. Finally, LY determination in the supernatant was performed by evaluating the absorbances of both

standards and samples at 450 nm using a microplate reader (BIORAD model 680, Hercules, CA, USA).

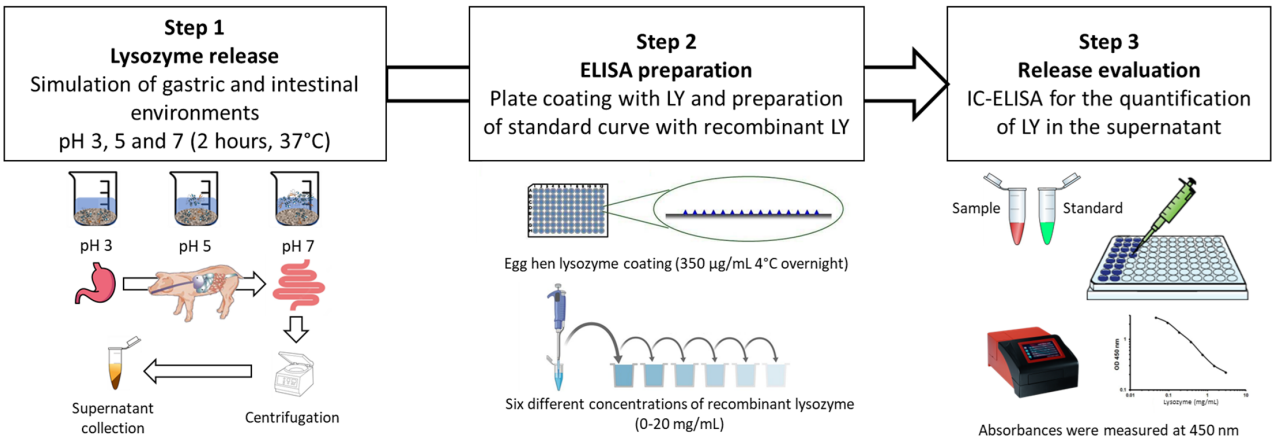

Figure 2. Steps in the procedure for the lysozyme release assay.

3. Results

3.1. Lysozyme and Carriers' Characterization

3.1.1. Lysozyme Characterization

A sample of pristine lysozyme (LY) was characterized with the combination of X-ray powder diffraction (XRPD), Fourier-transform infrared spectroscopy in attenuated total reflection mode (FT-IR-ATR mode), and thermogravimetric analysis (TGA). The results are plotted in Figure 3a–d.

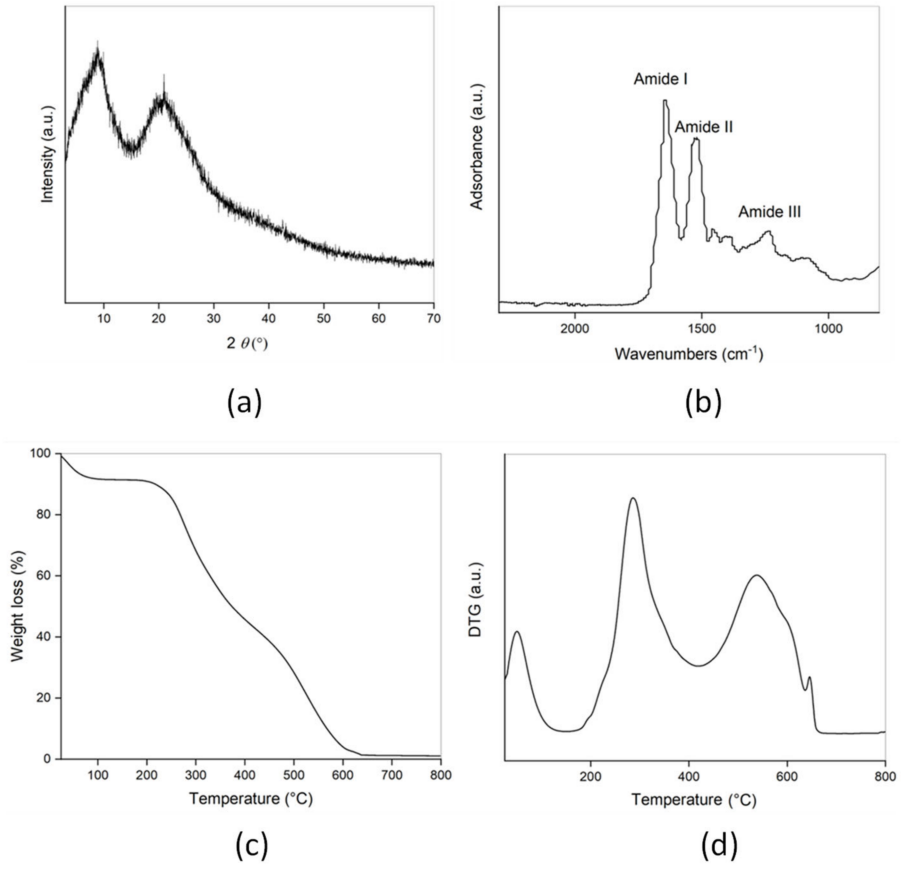

Figure 3. Pristine LY characterization (**a**) XRPD, (**b**) FT-IR-ATR, (**c**) TG, and (**d**) DTG analysis.

The XRPD pattern (Figure 3a) shows that LY is amorphous and, except for the two broad reflections at about 9 and 21 2θ°, no other reflections are detectable [11].

In Figure 3b, the FTIR-ATR spectrum of the protein is shown in the wavenumber region corresponding to the peptide linkage bands. The three main bands at 1643, 1523, and around 1300 cm^{-1} were assigned, respectively, to vibrational mode Amide I (mainly C=O stretching vibration), Amide II (mainly a combination of N–H in plane bending vibration and CN stretching mode), and Amide III (a combination of NH bending and CN stretching vibration) [11,27]. The analysis of the interaction between the protein and the inorganic matrix discussed next will focus on changes in the intensity and position of these diagnostic bands.

A total weight loss was found in the 30–700 °C temperature range (Figure 3c).

The DTG curves (Figure 3d) showed three regions of weight loss. The first thermal phenomenon (23–100 °C) is attributed to physiosorbed water loss, according to LY hygroscopic properties. The second larger weight loss, in the temperature range of 200–600 °C with a maximum at 300 °C, can be ascribed to the lysozyme decomposition. Finally, the last phenomenon at 600–800 °C is probably due to the decomposition of the last organic residues [28].

3.1.2. Carrier Characterizations

As potential LY carriers, two clay minerals and a zeolite-based material were tested. Morphological analysis was performed to evaluate pore dimensions, while determination of Zero Point Charge was carried out to better understand the surface properties and adsorptive capability of the selected carriers [29].

The results of the morphological analyses and Zero Point Charge values (ZPC) of pristine bentonite (BN), sepiolite (SP), and Phil 75® (PH) are summarized in Table 1.

All the materials are characterized by a trimodal distribution of the particle's dimensions and negatively charged surfaces. Depending on the carrier, pore dimensions in the range of 4–110 nm were measured.

Table 1. Morphology (SA: surface area, VP: pore volume, DP: pore diameter) and Zero Point Charge (ZPC) of the carriers. (BN: bentonite, SP: sepiolite, PH: Phil 75®.).

Carrier	SA (m^2/g)	VP (cm^3/g)	DP (nm)	Particle Dimension (μm)	ZPC (mV)
BN	28	0.07	12	2, 10, 35	−4.73
SP	78	0.14	5, 110	0.2, 2, 10	−122
PH	131	0.03	4	2, 20, 85	−169

The XRPD patterns of the pristine materials are reported in Figure 4. Bentonite (BN) mainly consists of montmorillonite [ICSD 98-016-1171], illite [ICSD 98-016-6962], chlorite [ICSD 98-006-8942], and albite [ICSD 98-007-7422], while sepiolite (SP) contains sepiolite [ICSD 98-018-2394] and dolomite [ICSD 98-017-1513]. Phil 75 (PH) consists of a mixture of zeolites, namely phillipsite [ICSD 98-005-1639], chabazite [ICSD 98-016-9579], and zeolite [ICSD 98-028-1762]; the additional reflections at about 28° 2θ are characteristic of feldspar [ICSD 98-008-6339]; a minor quartz component [ICSD 98-000-0174] is also present.

In Figure 5, the ATR-FT-IR spectra of the three studied samples are reported. In detail, the high-frequency region (Figure 5a) shows a broad absorption band extending from 3800 to 3000 cm^{-1}, affected by remarkable band overlapping. The latter is particularly severe in the PH and SP samples, thus preventing band assignment. In the case of BN, a well-defined and sharp band at 3620 cm^{-1}, with a shoulder at 3695 cm^{-1}, is ascribed to the stretching vibrations of structural OH groups, whereas bands at a lower wavenumber are due to the interlayer and adsorbed H_2O stretching vibrations, such as in montmorillonite spectrum [30–32]. In the range of 950–800 cm^{-1}, weak bands are due to AlAlOH and AlMgOH bending vibrational modes, while the main maximum is centered at 985 cm^{-1} and attributed to Si-O vibrational modes. Other absorption bands below 550 cm^{-1} belong to Si-O-Al and Si-O-Si deformation modes.

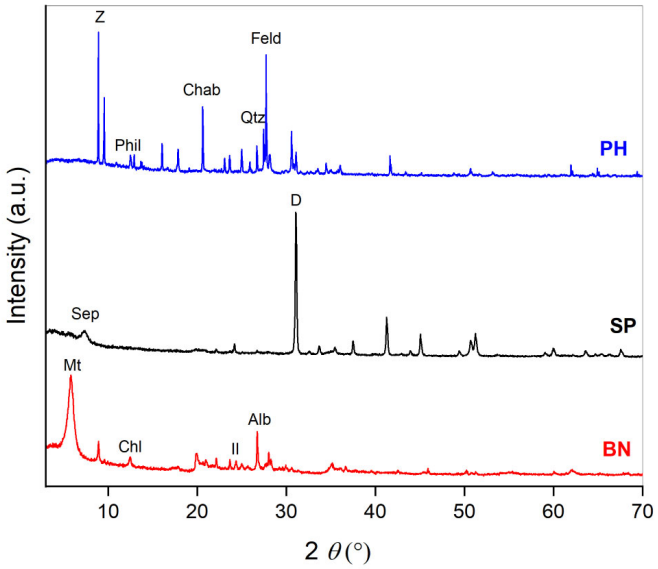

Figure 4. X-ray diffraction patterns of the carriers: bentonite (BN), sepiolite (SP), and Phil 75® (PH). The position of the most intense (I_{100}) peak of the single phases is reported. (Mt: montmorillonite, Il: illite, Chl: chlorite, Alb: albite, Sep: sepiolite, Chab: chabazite, Phil: phillipsite, Z: zeolite, Feld: feldspar, Qtz: quartz, D: dolomite).

In SP, in addition to the complex band centered at 995 cm^{-1} and due to Si-O vibrational modes, few minor components below 600 cm^{-1} are related to Si-O-Si deformations and OH deformation modes. Similarly, for Phil 75®, bands in the range of 1200–700 cm^{-1} (Si-O, Al-O, Si-O-Al vibrations) and below 650 cm^{-1} (Si-O-Al deformation modes) occur. A very weak absorption extending from 3700 to 3200 cm^{-1} is due to the stretching modes of OH groups, such as Si-OH, interacting through H-bonds. It is worth noticing that this material shows the weakest and ill-defined bands in this region of the spectrum [33,34]. Finally, a large band cantered at 1433 cm^{-1} and two sharper bands at 880 and 730 cm^{-1} in the spectrum SP, and assigned to carbonate species, are related to dolomite also detected by XRPD analysis.

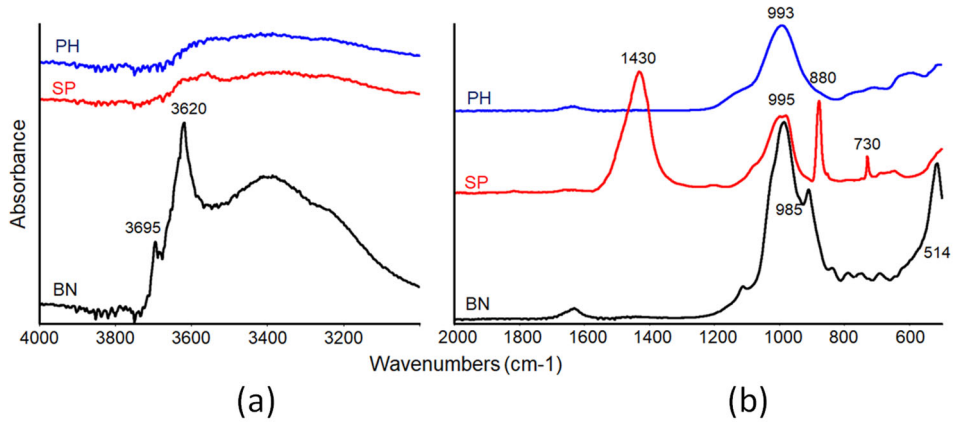

Figure 5. ATR FT-IR spectra of pristine materials: (**a**) enlargement of the high-frequency region, and (**b**) low-frequency region.

Pristine carriers were also characterized by TG (Figure S1); the experiments were conducted in air in the 25–800 °C temperature range. A total weight loss of about 13% for BN, 40% for SP, and 15% for PH was measured in these conditions.

By DTG analysis, it is possible to analyze the thermal phenomena associated with the observed weight losses; the DTG curves are plotted in Figure 6.

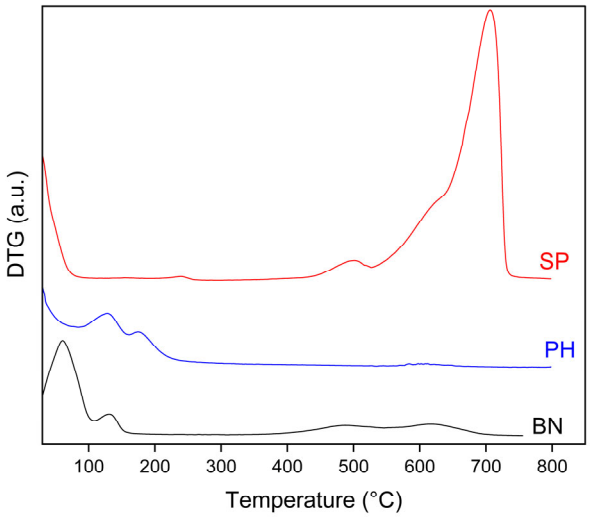

Figure 6. DTG curves of pristine carriers: bentonite (BN), sepiolite (SP), and Phil 75® (PH).

In the DTG curves of all the carriers (Figure 6), a thermal phenomenon, occurring between 25 and 100 °C, is manifested and consistent with the release of physiosorbed water molecules. Weight losses of about 4%–5% were detected for SP e PH, and of about 7% for BN. The slightly higher weight loss of the BN sample can be due to a possible hygroscopicity of this material.

On increasing the temperature, the BN sample shows a thermal phenomenon at about 130 °C (weight loss 1.4%), which can be due to the interlayer water release, while the further thermal effects in the range of 400–700 °C, barely manifested, account for dehydroxylation [35]. In the SP sample, the phenomenon at about 500 and 650 °C is related to dehydration, while that at about 750 °C is associated with the loss of OH groups [35].

Finally, in the case of the PH sample, the two phenomena at about 130 and 180 °C, for a total weight loss of about 10%, can be related to zeolitic and crystalline water release [35].

3.2. Study of the Adsorption Operating Parameters

The operating conditions to anchor the lysozyme to the carriers, via the solid/liquid adsorption procedure proposed here were studied in terms of reaction time, pH, and LY concentration in the initial solutions.

3.2.1. Effect of Reaction Time

The reaction time was evaluated by fixing the initial LY content at 37.5 $mg_{LY}/g_{carrier}$ [21], and performing the experiments at pH 4.3, i.e., without any pH correction. The solid–liquid reaction was performed by contacting the different carriers at different times, namely in the range of 10–90 min. Each carrier was contacted with the solution, and stirred for the fixed time, then the reaction was stopped, solid and liquids were separated, and the liquid was analyzed by COD.

For all the carriers, and for all the explored pH range, a constant LY capture was found, which corresponded to 37 mg/g in the case of SP, 33 mg/g in the case of BN, and 12 mg/g in the case of PH (Figure S2). Considering that stirring time does not influence the reaction yield, the reaction time was fixed at 30 min, for all the further experiments.

3.2.2. Effect of pH

In addition, the effect of pH was studied, in the range of 2–11.3, by fixing LY initial content at 37 $mg_{LY}/g_{carrier}$, and the reaction time at 30 min. It has been reported that the LY isoelectric point (IP) is influenced by pH and ionic strength [36,37], as well as clay and zeolite capture capability [38]. Therefore, the experiments were performed at pH = 2 and pH = 11.3, i.e., far below and near the IP [36]; moreover, a pH = 4.3 was also considered, being the natural pH of the initial LY solutions (Figure S3). For BN and PH, a slightly lower

LY capture occurs at pH = 2, which readily increases to reach a plateau value of 37 for BN and 12 $mg_{LY}/g_{carrier}$ for PH, at a pH = 4.3. On the contrary, no pH effect was observed on the SP carrier, where a constant LY loading of 37 mg_{LY}/g_{SP} was measured in the entire experimental range.

No significative effect of pH on LY adsorption onto a model clay surface was already reported for atomic force spectroscopy (AFM) investigation. In the investigated pH range (pH = 4–9), LY always showed a net positive charge, which made the protein strongly adsorbed at the negatively charged surface [1].

Accordingly, the pH of the further experiments was set at 4.3, without any modification of the natural pH of the LY initial solution.

3.2.3. Effect of Lysozyme Concentration

The dependence of the LY loading as a function of the initial LY concentration in solution was investigated in the range of 0.25–3.0 mg_{LY}/mL (corresponding to 6.25–75 $mg_{LY}/g_{carrier}$); 30 min of reaction time and pH = 4.3 were applied.

The results are plotted in Figure 7.

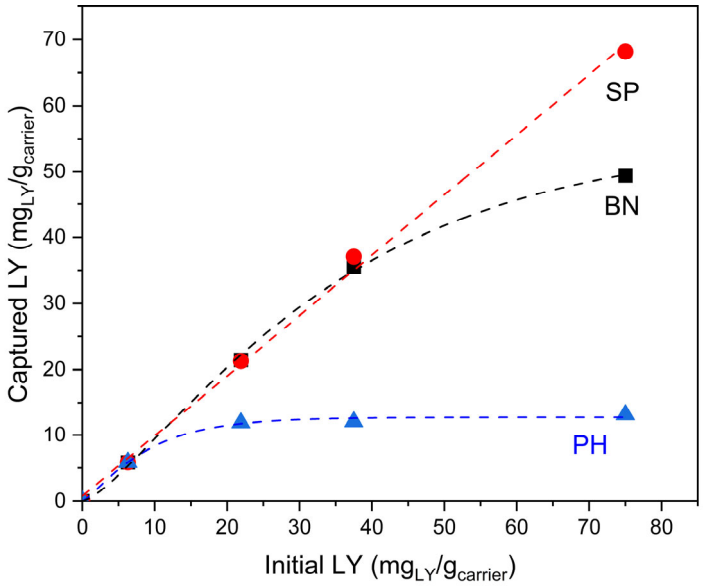

Figure 7. LY uptake as a function of initial LY content in contacting solutions.

A different behavior for the carriers was manifested; indeed, while for PH a plateau was already reached at 20 $mg_{LY}/g_{carrier}$ of LY initial content, for both BN and SP, a linear and overlapped capture behavior was observed up to an LY initial content of 37.5 $mg_{LY}/g_{carrier}$. Such a linear dependence was maintained in the SP carrier across the explored range; on the contrary, in BN a tendency to a plateau was manifested. Therefore, when the initial LY content was fixed to 37.5 $mg_{LY}/g_{carrier}$, a reaction yield of 100% could be obtained for BN and SP, while this was only 32% in the case of PH.

3.3. LY–Carrier Hybrid Materials Characterization

LY–carrier materials were fully characterized by means of different techniques; the final purpose was to understand LY allocation on the carrier, the nature, and the strength of the LY–carrier interactions. Indeed, these parameters can influence the release behavior of the materials under in vitro and in vivo conditions.

Moreover, a better knowledge of the system is helpful in the optimization of both the synthesis process and materials. The XRPD patterns of the studied hybrid materials do not show evidence of significant changes in comparison with the pristine carriers (Figure S4). It is known that the capacity of proteins to be adsorbed on clay minerals depends on several parameters such as pH of the solution, temperature, crystal chemical properties

of the mineral (cation exchange capacity, surface area, nature of the cation saturating the clay, etc.), isoelectric point, and size of the proteins [10,39]. More specifically, interlayer cations of montmorillonite affect its capability to interact with small polar molecules and stabilize proteins. For instance, homoionic Na^+-montmorillonite has a higher affinity in the adsorption of proteins with respect to its Ca^{2+}-counterpart [10]. The authors found that before the protein adsorption, the (001) diffraction peak in the X-ray diffraction pattern of homoionic Na^+- and Ca^{2+}-Mt is located at 2θ~9° and 7°, respectively, corresponding to an interlayer spacing (d_{001}) of 12 and 13.6 Å, respectively. After the protein adsorption, the interlayer spacing is ~54 Å for lysozyme/Na^+-Mt and up to 49 Å for lysozyme/Ca^{2+}-Mt. Similar results were found by Balme et al. [11]. A Δ d_{001} of ~10 Å was reported for other Na^+-Mt and explained invoking the intercalation of unfolded lysozyme [40]. The adsorption of lysozyme on other clay minerals (saponite) results in interlayer expansion to d_{001} of 44 Å 38 [39].

In our case, the (001) diffraction peak was observed at 2θ = 5.83° and 7.41° corresponding to 15.14 and 11.9 Å d_{001} spacing in BN and SP samples, respectively (Figure S4). These peaks do not display shifts toward lower 2θ angles after the interaction with the lysozyme (BN-LY and SP-LY patterns in Figure S4).

The ATR FT-IR subtraction spectra of hybrid materials are shown in Figure 8a,b, together with the spectrum of pure LY for comparison.

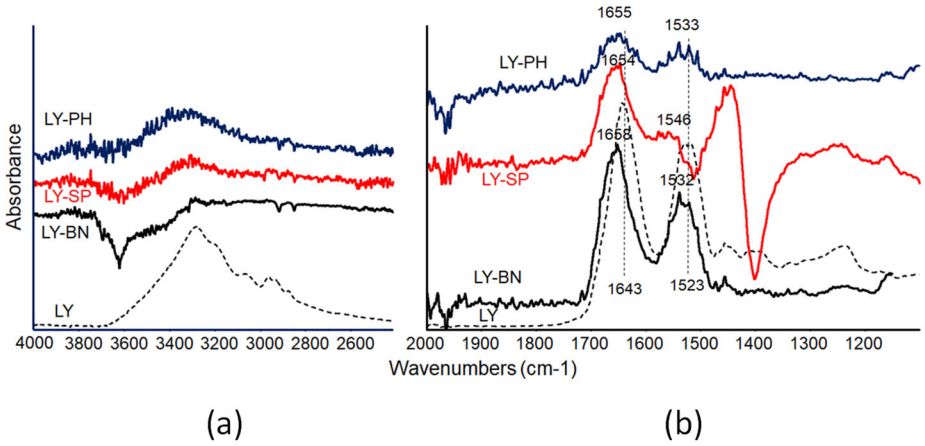

Figure 8. ATR FT-IR subtraction spectra of hybrid materials: (**a**) high-frequency region, (**b**) low-frequency region. Spectrum of pristine clay has been subtracted. Dashed line: pure LY spectrum.

In the high-frequency spectral region, the weak absorptions between 3400–3200 cm^{-1} correspond to N-H stretching vibrations, which is still detectable after adsorption [41]. The detection of negative bands centered around 3620 cm^{-1} confirms the involvement of the surface OH groups of clays with the organic moiety, and this effect is more evident in the BN sample spectrum.

Focusing on the main IR features in the low-frequency spectral region, in all the spectra of the hybrid materials Amide I and Amide II bands (located at 1643 and 1523 cm^{-1} in the spectrum of pure LY) appear broader and slightly shifted towards higher frequencies, i.e., 1658–54 and 1546–32 cm^{-1}, respectively, after immobilization in the solid matrix (Figure 8b). The analysis of the IR spectra of the mechanical mixture (Figure S5) showed evidence that in this case, the amide bands are detected at wavenumbers closer to those of the pure LY bands. This effect can be explained considering that in the hybrid materials, the spreading of the LY molecules on the clay surface will lead to the formation of H-bonds between the LY and clay surface sites and, on the other side, will break the intermolecular H-bonds among molecules in the pristine protein. Apparently, the integrity of the amide bond is not affected by the interaction and an increased loading of the protein, for instance, the BN-based sample corresponds to an increased intensity of these bands, in agreement with TG results discussed below. Moreover, in the spectrum of the sepiolite-based com-

posite, a significant negative band is detected near 1400 cm^{-1}, suggesting that carbonate species are perturbed during the synthesis procedure.

TG (figure not reported) was also performed, to find confirmation on LY loading on the solid.

To evaluate the LY loading in the hybrid materials, the weight losses in the range of LY decomposition (200–645 °C) were evaluated by subtracting the weight loss of the pristine carrier in the same range (Equation (2)).

$$\text{LY loading} = [(\text{LY-carrier weight loss}) - (\text{Pristine Carrier weight loss})] \quad (2)$$

The results of the calculation were then compared to COD results. For all the samples, a good correspondence was found between the LY content determined by the two independent techniques. Indeed, LY contents by TGA were 33 $mg_{LY}/g_{carrier}$ in the case of BN, 30 $mg_{LY}/g_{carrier}$ in the case of SP, and 11 mg/g in the case of PH; to be compared with those found by COD of 35.5 mg/g in case the of BN, 37 mg/g in the case of SP, and finally 12 mg/g in the case of PH.

To allow for a better evaluation of the samples' decomposition behavior, and to better understand the LY–carrier interactions' mechanism and strength, DTG analyses were also performed (Figure 9c).

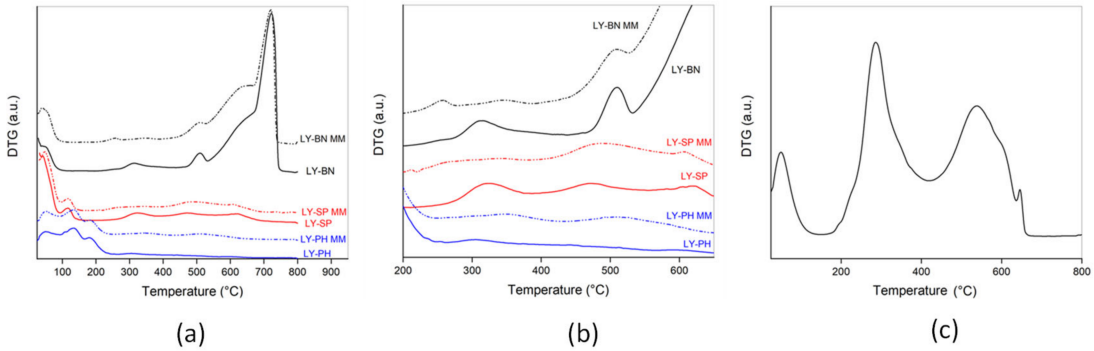

Figure 9. Comparison of DTG curves of hybrid materials and mechanical mixtures. (**a**) Temperature range 25–800 °C, (**b**) temperature range 200–650 °C, and (**c**) DTG of pristine LY reported for sake of comparison.

The barely evident phenomenon observed in all the hybrid materials (Figure 9a,b) can be the result of LY decomposition, which is reported in pristine LY at the same temperature range, with a maxima at 300 and 550 °C (Figure 9c); the other observed phenomena are due to clay and zeolite decomposition. The presence of LY decomposition residues which re-adsorb and thus decompose at higher temperatures cannot be discarded.

Although difficult to be detected, there appears to be a broadening of the phenomenon centered at 300 °C, accompanied by a slight shift of the maximum towards higher temperatures, more appreciable in the BN sample when the DTG scale is expanded (Figure 9b). Unfortunately, the marked decomposition at about 550 °C in pristine LY can hardly be seen in the hybrid samples, being overlapped to the carrier thermal phenomena or spread all over the temperature range. However, considering both the broadening and shift of the first decomposition, a somewhat LY–carrier interaction can be assumed.

To further investigate this point, three mechanical mixtures containing 37.5 $mg_{LY}/g_{carrier}$ (MM, in the following) were prepared, by grinding in a mortar of 0.075 g of LY and 2 g of each carrier. These samples were then subjected to TG and DTG analysis and the results were compared with the hybrid materials. In the mechanical mixtures, the LY decomposition is more evident (Figure 9a,b dashed lines) and it occurs at temperatures closer to those of free LY (Figure 9c), as if there were no interactions or very weak interactions.

To investigate LY location onto the carrier, SEM analyses were performed on both the hybrid materials and the mechanical mixtures. SEM images, taken at the same magnification of 2 μm, are reported in Figure 10 (pristine materials reported for sake of comparison).

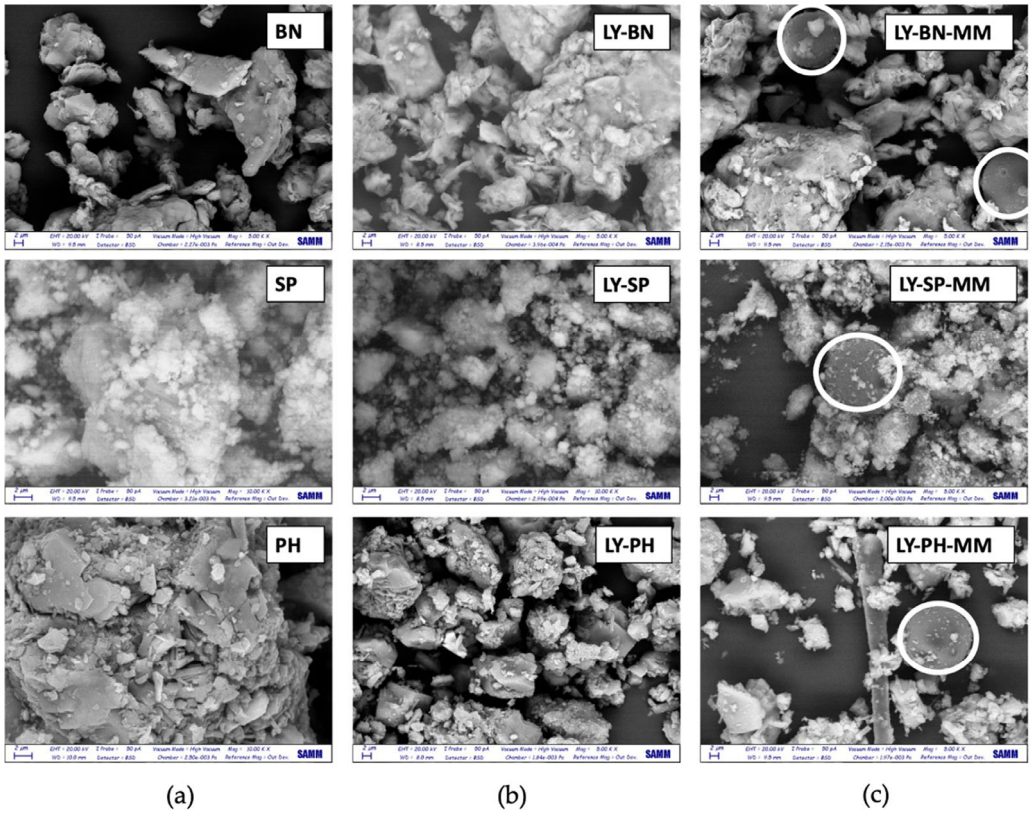

Figure 10. SEM images of (**a**) pristine carriers, (**b**) hybrid materials, and (**c**) mechanical mixtures (circles: LY particles) (magnification: 2 μm).

The pristine materials exhibit a complex morphology (Figure 10a), characterized by both large and small aggregates, which are still predominant in the LY–carrier hybrid samples (Figure 10b), suggesting a high LY dispersion in the sample. LY dispersion in hybrid materials was also confirmed by EDX analysis (Figure 11), where sulphur (S) atoms were used as tracers. Indeed, in the hybrid samples, a homogeneous distribution of S atoms on the whole sample is evident.

Largely different is the situation of the mechanical mixtures, where spherical particles and carrier features are co-present and clearly distinguishable (Figure 10c). In this case, S atoms are mainly confined in the spherical particles (Figure 11b,d); hence, it can be concluded that spherical aggregates consist of the undispersed LY weakly interacting or not interacting with the carrier at all. It must be underlined that no aggregates were distinguishable in the hybrid samples (Figures 10b and 11a,c).

This picture is also consistent with the DTG reports, where a stronger LY–carrier interaction was found in the hybrid samples, but not in the mechanical mixtures. The presence of stronger or weaker interactions would influence both protection capability of the three carriers towards the LY molecules, as well as the LY release during application.

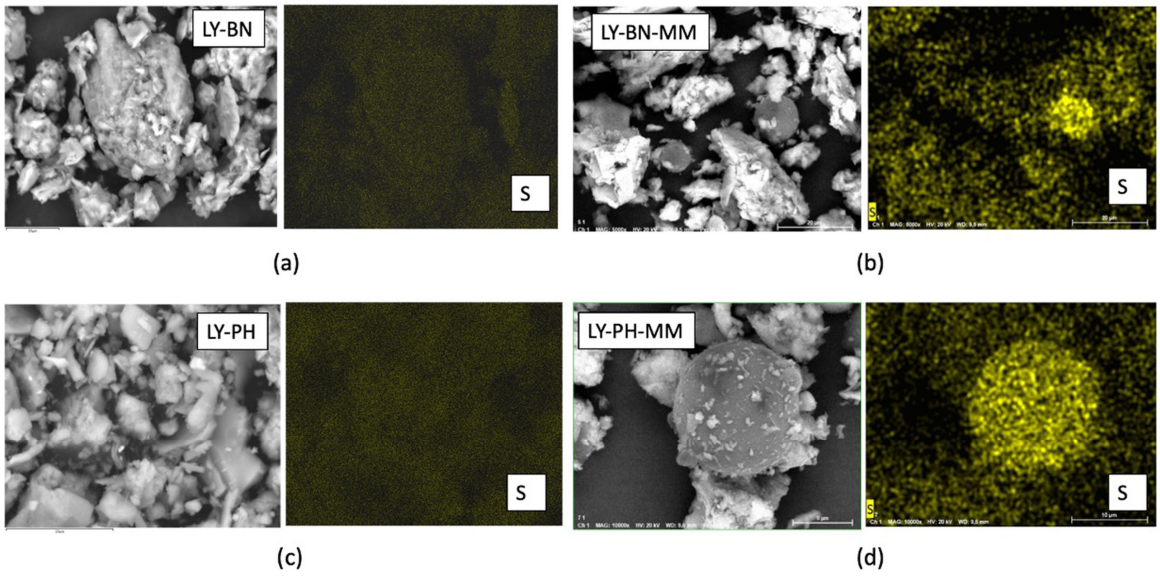

Figure 11. Comparison of SEM-EDX of (**a**,**b**) LY-BN, LY-BN-MM, and (**c**,**d**) LY-PH, LY-PH-MM. (SEM of the analyzed portions reported for sake of clarity, S = sulphur.).

3.4. Lysozyme Release Assay

Release tests were performed on the hybrid materials, LY-SP, LY-BN, and LY-PH and on the respective mechanical mixtures, under experimental conditions to simulate the pH conditions of stomach and intestine weaning pigs; the results are reported in Table 2.

For BN-LY and PH-LY, the lowest release was detected at pH 3, while the LY-SP sample showed an almost constant but larger release throughout the explored pH range. At pH 7, an LY release of 0.06–0.07 $mg_{LY}/g_{carrier}$ was measured for all the hybrid materials (Table 2). Compared to the hybrid materials, similar or slightly higher LY releases were found for LY-BN-MM and LY-SP-MM, while a much larger release was measured for LY-PH-MM. The calculated total percentage of released LY was about 0.3%–0.5% for BN- and SP-based samples, both hybrid samples and mechanical mixtures, while it was 1 and 4% for LY-PH and LY-PH-MM, respectively.

Table 2. LY release of hybrid materials and mechanical mixtures at different pHs. (LY: lysozyme, BN: bentonite, SP: sepiolite, PH: Phil75®, MM: mechanical mixture).

Sample	LY Loading ($mg/g_{carrier}$)	Release ($mg_{LY}/g_{carrier}$) @ pH 3	Release ($mg_{LY}/g_{carrier}$) @ pH 5	Release ($mg_{LY}/g_{carrier}$) @ pH 7	Total Release ($mg_{LY}/g_{carrier}$)	Total Release (%)
LY-BN	35	0.03	0.02	0.06	0.1	0.3
LY-BN-MM	37	0.02	0.02	0.07	0.11	0.3
LY-SP	37	0.06	0.06	0.07	0.19	0.5
LY-SP-MM	37	0.04	0.05	0.05	0.14	0.4
LY-PH	12	0.01	0.05	0.06	0.12	1
LY-PH-MM	37	0.1	0.7	0.64	1.44	4

4. Discussion

4.1. Materials Synthesis and LY Capture Mechanism

The synthetic approach reported here, i.e., solid–liquid adsorption, is simple, environmentally friendly, and effective for preparing hybrid materials characterized by considerable LY loadings. The result is dependent on the synthesis parameters, mainly the LY initial concentration and pH, but also, on the carrier nature.

Carrier characteristics, such as morphology and Zero Point Charge (ZPC), appear to be the driving force for an effective LY adsorption; as a matter of fact, both pore dimensions and ZPC can markedly affect the adsorption process.

Considering our samples, the effect of the ZPC is clear, the maximum LY capture already occurred after 10 min of reaction, and adsorptions lower than the maximum were only detected at pH = 2. All these data point to a very fast adsorption reaction, where the driving force is the surface charge. Indeed, the negatively charged surfaces of the carriers (ZPC of −169 mV for PH, −122 (mV) for SP, and −4.73 (mV) for BN) are highly prone to interact with the LY molecules, positively charged in this condition [36,39]. The lower adsorption observed at pH = 2, for BN and PH, can be due to a competition between protons, smaller and thus quicker, and the larger LY molecules (average volume of 169 nm^3 [42]). Therefore, considering this picture, the effect of the carrier ZPC appears predominant.

However, ZPC and charge interactions are not enough to explain the different adsorption extents observed for the carriers; that means 32% for PH and almost 100% for BN and SP. The PH surface, indeed, is the most negative one; therefore, the interaction of charges of opposite signs is expected to be highly favored, thus resulting in a larger LY capture. Accordingly, additional effects, such as surface morphology and pore dimensions, or the presence of surface groups of a different nature, or steric hindrance of LY molecules, must be considered, too. In this respect, this picture is in line with simulation results on lysozyme adsorption onto a charged solid surface, reported in the literature by other authors [1,8]. Indeed, it has been reported that, despite the electrostatic forces being found to play a key role in the LY–carrier binding process, such forces are unable to provide a full understanding of the interaction mechanism.

Coming to morphology, in PH zeolite, pores with a size of 4 nm are present, to be compared with the ellipsoidal LY dimensions of 4.5 × 3.0 × 3.0 nm, corresponding to a volume of 169 nm^3 [42]. It is evident that pores with a diameter of 4 nm are hardly able to host the large LY molecules. Different is the case of SP, the sample showing the maximum LY loading, where a bimodal distribution of the pores' diameter (5 nm and 110 nm) is present. The smaller pores can hardly be occupied by the LY molecules, while on the contrary, the larger pores could host the LY ellipsoidal molecules. Additionally, in the case of BN, pore diameters of 12 nm are consistent with the presence of LY molecules allocated in the pores. By considering the LY capture of the three carriers, 37 $mg_{LY}/g_{carrier}$ for LY-SP, 35 $mg_{LY}/g_{carrier}$ for LY-BN, and 12 $mg_{LY}/g_{carrier}$ for LY-PH, the combination of ZPC and morphology could explain carrier capture capability. Indeed, considering PH morphology, DP = 4 nm and ZPC (−169 mV), charge interaction appears to be the only possible binding mechanism; no LY can be hosted in the pores, due to their small dimensions. Hence, all the LY molecules are adsorbed at the surface, thus prone to steric hindrance and charge repulsion, resulting in the lowest LY capture. In the case of BN, the effect of the low ZPC could be compensated for by the large pore dimensions able to allocate LY molecules. Moreover, in the case of BN, an expandable clay, an exchanging mechanism implying interlayer cations, could also be possible, in principle.

The presence of an exchanging mechanism can be verified by following the Ca^{2+} ion release upon contact with the LY solution; indeed, if an exchanging mechanism is present, Ca^{2+} ions should be involved in the process [43,44], thus Ca^{2+} becoming the tracer of the exchange reaction. Accordingly, BN was treated with distilled water at pH = 4, and the released Ca^{2+} was compared with that measured in the presence of LY at the same pH. Released Ca^{2+} ions equal to 0.12 mg/g_{AD} were found in the experiment with pure water, while those equal to 0.28 mg/g_{BN} were measured for the LY-containing solution (35 mg/g_{BN}). Therefore, the hypothetical LY involved in the exchange reaction should correspond to the difference between released Ca^{2+} ions (0.003 $mmol_{Ca}/g_{BN}$) in water and released Ca^{2+} ion during the reaction (0.007 $mmol_{Ca}/g_{AD}$). Hence, by hypothesizing a 1:1 exchange and multiplying the Ca^{2+} mmoles (0.004 $moles/g_{BN}$) released during the reaction for the LY MW (14.4 kDa), an intercalated LY content of 0.576 mg_{LY}/g_{BN} should be present.

However, LY intercalation in the BN-based sample seems to not be supported by the XRPD analysis [11], since no significant shift in the position of the basal reflection (d_{001}) has been detected in the LY-BN XRPD pattern. Although limited, LY intercalation should be manifested due to the large LY dimensions, as it should result in the interlayer enlargement. On the other hand, dynamic modelling simulation studies on expandable clays, such as montmorillonite, revealed that the (010) edge surface is more chemically reactive than the basal one, being characterized by more hydroxyl groups, that can participate in acid/base chemistry during LY adsorption [9], and this explanation could be applied to our samples, too. In our experimental conditions, this hypothesis is also supported by IR results [30–34,41] showing that exposed OH groups are involved in the interaction between clay and the protein, particularly in the case of the BN matrix. However, surface adsorption is predominant on the other LY capture mechanisms.

Finally, in the case of SP, the highest LY capture is justified by a synergic combination of surface charge and pore dimensions. As a matter of fact, the IR spectrum of this sample shows very weak bands in the OH stretching region, suggesting a limited amount of "free" hydroxy groups available for adsorption processes. This behavior could be related to the presence of carbonate species, detected by FT-IR, which could modify the nature of the surface, and consequently the adsorption mechanism.

4.2. LY–Carrier Interaction Strength

The LY–carrier interaction is fundamental for the final application; LY distribution on the carrier and LY–carrier bond strength are of paramount importance to control the LY release during the gastric passage.

The synthetic approach applied here allowed for bonding the LY molecules to the carrier in a stronger way than in a simple mixture. This statement is supported by DTG analysis of the hybrid materials, where LY decomposition occurs at temperatures slightly higher than free LY, a clear indication of a LY–carrier interaction. These findings are also supported by DTG analysis of the mechanical mixtures, where, in turn, LY decomposition is detected at temperatures closer to those of free LY, thus suggesting no interactions or very weak interactions present in these samples [28].

This picture is also confirmed by SEM-EDX analysis of the hybrid materials, where LY molecules were found to be quite homogeneously spread onto the carriers' surface, being such a dispersion favored by the applied solid–liquid adsorption reaction. This was not the case with the mechanical mixtures, in which the mixed components (LY and carrier) were still clearly distinguishable in the SEM-EDX images. However, also for the MM samples, weak interactions due to surface charge can be inferred.

In the case of the proposed final application, i.e., feed optimization and bioactive molecule protection, the possibility to supply the bioactive molecules in a more controlled way is of paramount importance. However, the bioactive molecule, in this case LY, must preserve its properties in terms of structure and bioactivity.

When an immobilization process is applied, such as the solid–liquid adsorption proposed here, the occurrence of possible modifications in the protein structure upon binding must be evaluated. In large proteins, such as LY, it is the whole structure, indeed, that defines the active site configuration, in terms of exposed amino acid residues, thus the bioactivity.

Unfortunately, regarding structural changes in the LY upon adsorption, nothing can be said based on our results. In the hybrid samples, IR bands diagnostic of the peptide linkage are very weak and broad, and no other components can be detected. However, something can be hypothesized on the basis of the literature results on similar systems [1,8–10]. It has been reported, for Ca^{2+} montmorillonites [10], that the rigid hen egg white lysozyme is stabilized during adsorption, and no denaturation occurs. Furthermore, the electrostatic interactions, which guide the LY adsorption, are reported to steer the interaction of LY with the carrier surface via the N,C-terminal residues (for example, Arginine 128) of the protein chain.

This favorable binding orientation results in LY molecules being able to retain their secondary and tertiary structure, so that LY active site is not modified [8], and the bioactivity is preserved. Therefore, considering the close similarity between our systems and those reported in the literature, it can be hypothesized that a similar binding mechanism can occur in our samples, too. It can be assumed that, also with our carriers, LY is absorbed without denaturation, and thus able to retain its structure and function.

4.3. LY Release at Different pHs

Hybrid samples revealed a complex situation, in which some LY molecules were bonded in a weaker way with some others bonded in a stronger way. Accordingly, the release behavior could be markedly affected by the observed inhomogeneity.

On the other hand, differently bonded LY molecules could be prone differently to the pH effect, thus assuring their controlled released under the different gastrointestinal conditions.

Both hybrid samples and mechanical mixtures showed similar trends in LY release. All tested samples displayed a progressive higher LY release after increasing the pH level from 3 to 7 suggesting their use as possible carriers for the controlled release of LY in the gut. However, the different behavior of the carriers must be considered to select the most proper carrier for the application.

Regarding the carrier nature, BN-LY and PH-LY were more subjected to pH variations than SP. In view of their very little release at pH 3, but larger at pH 7, they appear to be better modulators for LY delivery in the application proposed here. Moreover, when BN- and SP-based materials are considered, their total release percentage 0.3–0.5% (w/w), makes these carriers probably adequate for a sufficient LY supply. Considering the observed release, an enhanced availability of the bounded lysozyme could be expected during the intestinal digestion due to the catabolic activity of pancreatic enzymes, bile salts, and the microbial population [45,46]. A slow and controlled release could guarantee the spreading of bioactive compounds carried by natural clays during the whole intestinal transit and modulating the microbiota population along the gut tract.

Interestingly, total LY release of 1 and 4% was found for LY-PH and LY-PH-MM, respectively. Furthermore, if the absolute value of the released LY is considered, i.e., 0.12 and 1.44 mg_{LY}/g_{PH} for LY-PH and LY-PH-MM, respectively, it appears that the mechanical mixture, LY-PH-MM, containing 37.5 mg_{LY}/g_{PH}, is the most promising sample to be used in the application.

As already remarked, lysozyme supplementation could be beneficial for the feed characteristics: it satisfies nutritional requirements, and, for its functional role, it protects animals and the resulting meat and dairy products from pathogenic bacteria (e.g., *Clostridium tyrobutyricum*) [47]. In addition, LY has been shown to increase zootechnical performance, animal welfare, and health, mainly influencing intestinal flora and nutrient digestibility [47–50]. Considering the obtained findings, even if the release rate was limited, the antimicrobial activity of LY could be targeted in the intestinal environment, to reduce pathogenic bacteria abundance, thus favoring the gut eubiosis and animal health.

5. Conclusions

The simple and environmentally friendly solid–liquid adsorption approach proposed here has been demonstrated to be effective for preparing hybrid materials for zootechnical applications.

LY initial concentration, pH, and carrier nature are the parameters of choice to manage LY loadings and interaction with different carriers. When the initial LY content is fixed to 37.5 $mg_{LY}/g_{carrier}$, with a reaction time of 30 min and pH at 4.3 (i.e., without pH correction), a 100% reaction yield can be obtained for BN and SP, while this is only 32% in the case of PH.

LY adsorption mainly depends on a combination of pore dimensions and Zero Point Charge. The absence of larger pores, able to allocate large LY molecules, is compensated for by the strong interaction between charges of opposite sign (i.e., positive LY–negative

carriers' surface). Depending on the carrier, the adsorbate, and the operating conditions, one of the two phenomena can prevail over the other. Surface hydroxy groups could also be involved in the interaction, in particular for the BN-based samples.

The interaction mechanism is the result of the preparation procedure: following the synthetic route, LY is homogeneously spread onto the carrier surface, and no separated LY aggregation is present in the material. On the contrary, LY aggregates are always present in the mechanical mixtures, although the interaction between charges of opposite signs is partially active, and also in the simple mixing of the component.

By comparing the results from our samples with the literature, it can be concluded that the electrostatic interaction mechanism results in a favorable binding orientation of the LY molecules, where the active sites are not modified, and the bioactivity is preserved.

The total release (0.3%–0.5% *w*/*w*) of BN-LY and PH-LY, combined with their response to the pH effect, make these carriers probably adequate for LY supply and modulation. Moreover, LY-PH and LY-PH-MM, due to their total LY release (1 and 4% w/w, respectively) are also interesting systems.

For all the samples, the observed higher release at pH 7 indicates their possible use as carriers for bioactive compounds to the intestinal environment possibly overtaking the gastric barrier.

The simple preparation route and an equally simple key to understand the interaction phenomena between the bioactive molecule and the carrier proposed here could facilitate the choice of the most appropriate carrier, being based on objective data, such as the carrier morphology or the carrier Zero Point Charge. Moreover, it should be noted that the study carried out in this work concerns samples prepared using commercial carriers, already applied in the feed industry as additives, and thus, it brings these materials closer to the market.

In fact, these clay-based systems for lysozyme delivery could provide a low-cost technology, in compliance with requests made by feed manufacturers, for market and livestock systems in the development of a targeted delivery of low concentrations of several bioactive compounds for the modulation of gut microbiota, intestinal health, and immune response.

Therefore, this study can constitute a step forward in the development of new optimized feed formulations for the targeted delivery of natural compound alternatives to antibiotics and vaccinal antigens.

Supplementary Materials: The following supporting information can be downloaded at: https://www.mdpi.com/article/10.3390/min13050660/s1, Figure S1: TG analysis of the pristine carriers: bentonite (BN), sepiolite (SP), and Phil 75® (PH); Figure S2: LY uptake as a function of reaction time; Figure S3: LY uptake as a function of pH; Figure S4: Comparison of XRPD patterns of pristine carrier, hybrid materials, and mechanical mixture for (a) BN-based, (b) SP-based, and (c) PH-based samples; Figure S5: ATR IR spectra of mechanical mixtures. Dashed line: pure LY.

Author Contributions: Conceptualization, M.G., C.C. and L.R.; methodology, M.G., S.R., M.D., M.L., E.M., C.C. and E.F.; validation, S.R., M.G. and M.D.; formal analysis, G.D., E.M. and E.S.; investigation, M.G., E.St., E.F. and S.R.; data curation, M.G. and E.St.; writing—original draft preparation, M.G., C.C., M.D. and E.F.; writing—review and editing, M.G., C.C., M.D., E.F., M.L., E.M., S.R., L.R. and E.S.; supervision, M.G. All authors have read and agreed to the published version of the manuscript.

Funding: This research received no external funding.

Data Availability Statement: Data are available upon request from the authors.

Acknowledgments: The authors acknowledge Biomicron s.r.l. (Reggio Emilia, RE, Italy) for providing carrier samples, and Giancarlo Selmini (Ferraroni SpA) for stimulating the discussion on carriers' selection. Thanks is also due to Mattia Ronchi (Politecnico of Milano, Dipartimento di Chimica, Materiali ed Ingegneria Chimica "Giulio Natta") and N. Mongelli (Università degli Studi di Bari Aldo Moro, Dipartimento di Scienze della Terra e Geoambientali) for their help in performing the scanning electron microscopy (SEM) and energy dispersion X-ray (EDX) analyses. The XRPD laboratory at the Dipartimento di Scienze della Terra e Geoambientali, Università degli Studi di Bari Aldo Moro

was funded by Potenziamento Strutturale PONa3_00369 "Laboratorio per lo Sviluppo Integrato delle Scienze e delle Tecnologie dei Materiali Avanzati e per dispositivi innovativi (SISTEMA)".

Conflicts of Interest: The authors declare no conflict of interest.

References

1. Kolman, K.; Makowski, M.M.; Golriz, A.A.; Kappl, M.; Pigłowski, J.; Butt, H.-J.; Kiersnowski, A. Adsorption, Aggregation, and Desorption of Proteins on Smectite Particles. *Langmuir* **2014**, *30*, 11650–11659. [CrossRef] [PubMed]
2. Watts, S.A.; Lawrence, A.L.; Lawrence, J.M. Chapter 10—Nutrition. In *Sea Urchins: Biology and Ecology*; Lawrence, J.M., Ed.; Developments in Aquaculture and Fisheries Science; Elsevier: Amsterdam, The Netherlands, 2020; Volume 43, pp. 191–208. [CrossRef]
3. 32003R1831, Regulation (EC) No 1831/2003 of the European Parliament and of the Council of 22 September 2003 on Additives for Use in Animal Nutrition. Available online: https://eur-lex.europa.eu (accessed on 17 March 2023).
4. Nadziakiewicza, M.; Kehoe, S.; Micek, P. Physico-Chemical Properties of Clay Minerals and Their Use as a Health Promoting Feed Additive. *Animals* **2019**, *9*, 714. [CrossRef] [PubMed]
5. Kaffash, E.; Shahbazi, M.-A.; Hatami, H.; Nokhodchi, A. An Insight into Gastrointestinal Macromolecule Delivery Using Physical Oral Devices. *Drug Discov. Today* **2022**, *27*, 2309–2321. [CrossRef] [PubMed]
6. Homayun, B.; Lin, X.; Choi, H.-J. Challenges and Recent Progress in Oral Drug Delivery Systems for Biopharmaceuticals. *Pharmaceutics* **2019**, *11*, 129. [CrossRef]
7. Cristiani, C.; Finocchio, E.; Rossi, L.; Giromini, C.; Dell'Anno, M.; Panseri, S.; Bellotto, M. Natural Clays as Potential Amino Acids Carriers for Animal Nutrition Application. *Appl. Sci.* **2021**, *11*, 5669. [CrossRef]
8. Kubiak-Ossowska, K.; Mulheran, P.A. What Governs Protein Adsorption and Immobilization at a Charged Solid Surface? *Langmuir* **2010**, *26*, 7690–7694. [CrossRef]
9. Andersen, A.; Reardon, P.N.; Chacon, S.S.; Qafoku, N.P.; Washton, N.M.; Kleber, M. Protein–Mineral Interactions: Molecular Dynamics Simulations Capture Importance of Variations in Mineral Surface Composition and Structure. *Langmuir* **2016**, *32*, 6194–6209. [CrossRef]
10. Lepoitevin, M.; Jaber, M.; Guégan, R.; Janot, J.-M.; Dejardin, P.; Henn, F.; Balme, S. BSA and Lysozyme Adsorption on Homoionic Montmorillonite: Influence of the Interlayer Cation. *Appl. Clay Sci.* **2014**, *95*, 396–402. [CrossRef]
11. Balme, S.; Guégan, R.; Janot, J.-M.; Jaber, M.; Lepoitevin, M.; Dejardin, P.; Bourrat, X.; Motelica-Heino, M. Structure, Orientation and Stability of Lysozyme Confined in Layered Materials. *Soft Matter.* **2013**, *9*, 3188–3196. [CrossRef]
12. Dell'Anno, M.; Scaglia, E.; Reggi, S.; Grossi, S.; Angelo Sgoifo Rossi, C.; Frazzini, S.; Caprarulo, V.; Rossi, L. Evaluation of Tributyrin Supplementation n Milk Replacer on Diarrhoea Occurrence in Pre-Weaning Holstein Calves. *Animal* **2023**, *17*, 100791. [CrossRef]
13. Ulbrich, K.; Holá, K.; Šubr, V.; Bakandritsos, A.; Tuček, J.; Zbořil, R. Targeted Drug Delivery with Polymers and Magnetic Nanoparticles: Covalent and Noncovalent Approaches, Release Control, and Clinical Studies. *Chem. Rev.* **2016**, *116*, 5338–5431. [CrossRef] [PubMed]
14. Hosseini, S.A.; Meimandipour, A. Feeding Broilers with Thyme Essential Oil Loaded in Chitosan Nanoparticles: An Efficient Strategy for Successful Delivery. *Br. Poult. Sci.* **2018**, *59*, 669–678. [CrossRef] [PubMed]
15. Lamphear, B.J.; Jilka, J.M.; Kesl, L.; Welter, M.; Howard, J.A.; Streatfield, S.J. A Corn-Based Delivery System for Animal Vaccines: An Oral Transmissible Gastroenteritis Virus Vaccine Boosts Lactogenic Immunity in Swine. *Vaccine* **2004**, *22*, 2420–2424. [CrossRef]
16. Papatsiros, V.G.; Katsoulos, P.D.; Koutoulis, K.C.; Karatzia, M.; Dedousi, A.; Christodoulopoulos, G. Alternatives to antibiotics for farm animals. *CABI Rev.* **2013**, *2013*, 1–15. [CrossRef]
17. Micuchova, A.; Piackova, V.; Frebort, I.; Korytar, T. Molecular Farming: Expanding the Field of Edible Vaccines for Sustainable Fish Aquaculture. *Rev. Aquac.* **2022**, *14*, 1978–2001. [CrossRef]
18. Wu, T.; Jiang, Q.; Wu, D.; Hu, Y.; Chen, S.; Ding, T.; Ye, X.; Liu, D.; Chen, J. What Is New in Lysozyme Research and Its Application in Food Industry?—A Review. *Food Chem.* **2018**, *274*, 698–709. [CrossRef]
19. Masschalck, B.; Van Houdt, R.; Haver, E.; Michiels, C. Inactivation of Gram-Negative Bacteria by Lysozyme, Denatured Lysozyme, and Lysozyme-Derived Peptides under High Hydrostatic Pressure. *Appl. Environ. Microbiol.* **2001**, *67*, 339–344. [CrossRef]
20. Ibrahim, H.; Aoki, T.; Pellegrini, A. Strategies for New Antimicrobial Proteins and Peptides: Lysozyme and Aprotinin as Model Molecules. *CPD* **2002**, *8*, 671–693. [CrossRef]
21. Oliver, W.T.; Wells, J.E. Lysozyme as an Alternative to Growth Promoting Antibiotics in Swine Production. *J. Animal Sci. Biotechnol.* **2015**, *6*, 35. [CrossRef]
22. Giromini, C.; Tretola, M.; Cristiani, C.; Finocchio, E.; Silacci, P.; Panseri, S.; Dell'Anno, M.; Baldi, A.; Rossi, L. Evaluation of the Absorption of Methionine Carried by Mineral Clays and Zeolites in Porcine Ex Vivo Permeability Models. *Appl. Sci.* **2021**, *11*, 6384. [CrossRef]
23. 5220 chemical oxygen demand (COD). In *Standard Methods for the Examination of Water and Wastewater*; American Public Health Association: Washington, DC, USA, 2017. [CrossRef]

24. O'Dell, J.W. Method 410.4 the determination of chemical oxygen demand by semi-automated colorimetry. In *Environmental Monitoring Systems Laboratory Office of Research and Development*; Revision 2.0; U.S. Environmental Protection Agency: Cincinnati, OH, USA, 1993. Available online: https://www.epa.gov/sites/default/files/2015-08/documents/method_410-4_1993.pdf (accessed on 17 March 2023).
25. Klank, D.; Goverde, T.; Blum, C. *Particle World*; Technical Papers of Quantachrome; QUANTACHROME: Klundert, The Netherlands, 2009; Available online: www.quantachrome.com (accessed on 17 March 2023).
26. Polakowski, C.; Ryżak, M.; Sochan, A.; Beczek, M.; Mazur, R.; Bieganowski, A. Particle Size Distribution of Various Soil Materials Measured by Laser Diffraction—The Problem of Reproducibility. *Minerals* **2021**, *11*, 465. [CrossRef]
27. Barth, A. Infrared Spectroscopy of Proteins. *Biochim. Biophys. Acta (BBA) Bioenerg.* **2007**, *1767*, 1073–1101. [CrossRef]
28. Elkordy, A.A.; Forbes, R.T.; Barry, B.W. Integrity of Crystalline Lysozyme Exceeds That of a Spray-Dried Form. *Int. J. Pharm.* **2002**, *247*, 79–90. [CrossRef]
29. Aghazadeh, V.; Barakan, S.; Bidari, E. Determination of Surface Protonation-Deprotonation Behavior, Surface Charge, and Total Surface Site Concentration for Natural, Pillared and Porous Nano Bentonite Heterostructure. *J. Mol. Struct.* **2020**, *1204*, 127570. [CrossRef]
30. Madejová, J.; Janek, M.; Komadel, P.; Herbert, H.-J.; Moog, H.C. FTIR Analyses of Water in MX-80 Bentonite Compacted from High Salinary Salt Solution Systems. *Appl. Clay Sci.* **2002**, *20*, 255–271. [CrossRef]
31. Slaný, M.; Jankovič, Ľ.; Madejová, J. Structural Characterization of Organo-Montmorillonites Prepared from a Series of Primary Alkylamines Salts: Mid-IR and near-IR Study. *Appl. Clay Sci.* **2019**, *176*, 11–20. [CrossRef]
32. Madejová, J.; Barlog, M.; Jankovič, Ľ.; Slaný, M.; Pálková, H. Comparative Study of Alkylammonium- and Alkylphosphonium-Based Analogues of Organo-Montmorillonites. *Appl. Clay Sci.* **2021**, *200*, 105894. [CrossRef]
33. Rykl, D.; Pechar, F. Thermal Decomposition of Natural Phillipsite. *Zeolites* **1991**, *11*, 680–683. [CrossRef]
34. Gualtieri, A.F. Study of NH_4^+ in the Zeolite Phillipsite by Combined Synchrotron Powder Diffraction and IR Spectroscopy. *Acta Crystallogr. B Struct. Sci.* **2000**, *56*, 584–593. [CrossRef]
35. Földvári, M. *Handbook of Thermogravimetric System of Minerals and Its Use in Geological Practice*; Occasional Papers of the Geological Institute of Hungary; Geological Institute of Hungary: Budapest, Hungary, 2011.
36. Kalburcu, T.; Tabak, A.; Ozturk, N.; Tuzmen, N.; Akgol, S.; Caglar, B.; Denizli, A. Adsorption of Lysozyme from Aqueous Solutions by a Novel Bentonite–Tyrptophane (Bent–Trp) Microcomposite Affinity Sorbent. *J. Mol. Struct.* **2015**, *1083*, 156–162. [CrossRef]
37. Najafi, A.; Sharifi, F.; Mesgari-Abbasi, S.; Khala, G. Influence of pH and temperature parameters on the sol-gel synthesis process of meso porous ZrC nanopowder. *Ceram. Int.* **2022**, *48*, 26725–26731. [CrossRef]
38. Chang, Y.-K.; Chu, L.; Tsai, J.-C.; Chiu, S.-J. Kinetic Study of Immobilized Lysozyme on the Extrudate-Shaped NaY Zeolite. *Process Biochem.* **2006**, *41*, 1864–1874. [CrossRef]
39. Johnston, C.T.; Premachandra, G.S.; Szabo, T.; Lok, J.; Schoonheydt, R.A. Interaction of Biological Molecules with Clay Minerals: A Combined Spectroscopic and Sorption Study of Lysozyme on Saponite. *Langmuir* **2012**, *28*, 611–619. [CrossRef] [PubMed]
40. Violante, A.; de Cristofaro, A.; Rao, M.A.; Gianfreda, L. Physicochemical Properties of Protein-Smectite and Protein-$Al(OH)_x$-Smectite Complexes. *Clay Miner.* **1995**, *30*, 325–336. [CrossRef]
41. Liltorp, K.; Maréchal, Y. Hydration of Lysozyme as Observed by Infrared Spectrometry. *Biopolymers* **2005**, *79*, 185–196. [CrossRef] [PubMed]
42. Cegielska-Radziejewska, R.; Lesnierowski, G.; Kijowski, J. Properties and Application of Egg White Lysozyme and Its Modified Preparations—A Review. *Pol. J. Food Nutr. Sci.* **2008**, *58*, 5–10.
43. Cristiani, C.; Iannicelli-Zubiani, E.M.; Dotelli, G.; Finocchio, E.; Gallo Stampino, P.; Licchelli, M. Polyamine-Based Organo-Clays for Polluted Water Treatment: Effect of Polyamine Structure and Content. *Polymers* **2019**, *11*, 897. [CrossRef]
44. Iannicelli-Zubiani, E.M.; Cristiani, C.; Dotelli, G.; Gallo Stampino, P.; Pelosato, R.; Mesto, E.; Schingaro, E.; Lacalamita, M. Use of Natural Clays as Sorbent Materials for Rare Earth Ions: Materials Characterization and Set up of the Operative Parameters. *Waste Manag.* **2015**, *46*, 546–556. [CrossRef]
45. Shahdadi Sardo, H.; Saremnejad, F.; Bagheri, S.; Akhgari, A.; Afrasiabi Garekani, H.; Sadeghi, F. A review on 5-aminosalicylic acid colon-targeted oral drug delivery systems. *Int. J. Pharm.* **2019**, *558*, 367–379. [CrossRef]
46. Kim, H.Y.; Cheon, J.H.; Lee, S.H.; Min, J.Y.; Back, S.Y.; Song, J.G.; Kim, D.H.; Lim, S.J.; Han, H.K. Ternary nanocomposite carriers based on organic clay-lipid vesicles as an effective colon-targeted drug delivery system: Preparation and in vitro/in vivo characterization. *J. Nanobiotechnol.* **2020**, *18*, 17. [CrossRef]
47. Dragoni, I.; Balzaretti, C.; Rossini, S.; Rossi, L.; Dell'Orto, V.; Baldi, A. Detection of Hen Lysozyme on Proteic Profiles of Grana Padano Cheese through SELDI-TOF MS High-Throughput Technology during the Ripening Process. *Food Anal. Methods* **2011**, *4*, 233–239. [CrossRef]
48. Ma, X.; Zhang, S.; Pan, L.; Piao, X. Effects of Lysozyme on the Growth Performance, Nutrient Digestibility, Intestinal Barrier and Microbiota of Weaned Pigs Fed Diets Containing Spray-Dried Whole Egg or Albumen Powder. *Can. J. Anim. Sci.* **2017**, *97*, 466–475. [CrossRef]

49. Abdel-Latif, M.A.; El-Far, A.H.; Elbestawy, A.R.; Ghanem, R.; Mousa, S.A.; Abd El-Hamid, H.S. Exogenous Dietary Lysozyme Improves the Growth Performance and Gut Microbiota in Broiler Chickens Targeting the Antioxidant and Non-Specific Immunity MRNA Expression. *PLoS ONE* **2017**, *12*, e0185153. [CrossRef] [PubMed]
50. Larsen, I.S.; Jensen, B.A.H.; Bonazzi, E.; Choi, B.S.Y.; Kristensen, N.N.; Schmidt, E.G.W.; Süenderhauf, A.; Morin, L.; Olsen, P.B.; Hansen, L.B.S.; et al. Fungal Lysozyme Leverages the Gut Microbiota to Curb DSS-Induced Colitis. *Gut Microbes* **2021**, *13*, 1988836. [CrossRef] [PubMed]